

RESEARCH

Open Access



Systematic interrogation of functional genes underlying cholesterol and lipid homeostasis

Haihuan Shan^{1,2,3}, Shuangshuang Fan^{1,2,3}, Quanrun Li^{1,2,3}, Ruipu Liang^{1,2,3}, Zhisong Chen^{1,2,3}, Shengnan Wang^{1,2,3}, Xiaofeng Wang^{1,2,3}, Yurong Li^{1,2,3}, Shuai Chen⁴, Kun Yu⁵ and Teng Fei^{1,2,3*}

*Correspondence:
feiteng@mail.neu.edu.cn

¹ Key Laboratory of Bioresource Research and Development of Liaoning Province, College of Life and Health Sciences, Northeastern University, Shenyang 110819, China

² National Frontiers Science Center for Industrial Intelligence and Systems Optimization, Northeastern University, Shenyang 110819, China

³ Key Laboratory of Data Analytics and Optimization for Smart Industry (Northeastern University), Ministry of Education, Shenyang 110819, China

⁴ Research Center for Analytical Sciences, Department of Chemistry, College of Sciences, Northeastern University, Shenyang 110819, China

⁵ College of Medicine and Bioinformation Engineering, Northeastern University, Shenyang 110819, China

Abstract

Background: Dyslipidemia or hypercholesterolemia are among the main risk factors for cardiovascular diseases. Unraveling the molecular basis of lipid or cholesterol homeostasis would help to identify novel drug targets and develop effective therapeutics.

Results: Here, we adopt a systematic approach to catalog the genes underlying lipid and cholesterol homeostasis by combinatorial use of high-throughput CRISPR screening, RNA sequencing, human genetic variant association analysis, and proteomic and metabolomic profiling. Such integrative multi-omics efforts identify gamma-glutamyltransferase GGT7 as an intriguing potential cholesterol and lipid regulator. As a SREBP2-dependent target, *GGT7* positively regulates cellular cholesterol levels and affects the expression of several cholesterol metabolism genes. Furthermore, GGT7 interacts with actin-dependent motor protein MYH10 to control low-density lipoprotein cholesterol (LDL-C) uptake into the cells. Genetic ablation of *Ggt7* in mice leads to reduced serum cholesterol levels, supporting an *in vivo* role of *Ggt7* during cholesterol homeostasis.

Conclusions: Our study not only provides a repertoire of lipid or cholesterol regulatory genes from multiple angles but also reveals a causal link between a gamma-glutamyltransferase and cholesterol metabolism.

Keywords: Lipid, Cholesterol, Gamma-glutamyltransferase, GGT7, CRISPR

Background

As the most abundant sterol in mammals, cholesterol plays many vital roles in both physiological and pathological conditions. It not only constitutes a major part of the eukaryotic cell membrane but also serves as precursors for many bioactive molecules such as bile acids and steroid hormones [1, 2]. In addition, cholesterol can also covalently bind to proteins (e.g., Hedgehog and Smoothed), thereby acting as critical regulators of key signaling pathways [3, 4]. Disturbed cholesterol or lipid homeostasis has been regarded as a major risk factor for atherosclerotic cardiovascular diseases as well as several neurodegenerative diseases and cancers [5, 6]. The levels of cholesterol



© The Author(s) 2025. **Open Access** This article is licensed under a Creative Commons Attribution-NonCommercial-NoDerivatives 4.0 International License, which permits any non-commercial use, sharing, distribution and reproduction in any medium or format, as long as you give appropriate credit to the original author(s) and the source, provide a link to the Creative Commons licence, and indicate if you modified the licensed material. You do not have permission under this licence to share adapted material derived from this article or parts of it. The images or other third party material in this article are included in the article's Creative Commons licence, unless indicated otherwise in a credit line to the material. If material is not included in the article's Creative Commons licence and your intended use is not permitted by statutory regulation or exceeds the permitted use, you will need to obtain permission directly from the copyright holder. To view a copy of this licence, visit <http://creativecommons.org/licenses/by-nc-nd/4.0/>.

within a cell are intricately orchestrated by a series of processes including biosynthesis, uptake, export, and esterification. Pioneering work have identified several key genes and signaling pathways underlying these processes and some of them have been targeted pharmacologically to treat cardiovascular diseases [2, 7–15]. For instance, HMGCR, the rate-limiting enzyme of cholesterol biosynthesis, is the central target for various statin drugs which can indirectly reduce serum low-density lipoprotein cholesterol (LDL-C) through a feedback regulation. PCSK9, a secreted protein that targets low-density lipoprotein receptor (LDLR) for lysosome degradation, stands for another successful target of therapeutic interventions to lower serum LDL-C and cardiovascular disease risks. Therefore, it is important and necessary to systematically identify the functional genes during cholesterol metabolism. Moreover, as research advances, a growing number of human genetic variants have been associated with cholesterol and lipid metabolism as well as cardiovascular diseases. However, a causal link needs to be established to pinpoint the functional genes underlying these physiopathological processes.

The application of clustered regularly interspaced short palindromic repeats (CRISPR)-based genome editing tools has significantly accelerated the pace of functional gene discovery, especially when combined with a high-throughput genetic screening approach [16–18]. CRISPR screening has been performed to identify the genes that regulate LDL-C uptake, LDLR or PCSK9 levels, HMGCR protein stability, SREBP signaling, and cholesterol trafficking using different screening platforms in various cellular models [19–28]. Several novel cholesterol regulators are characterized. On the other hand, the above studies usually focus on a specific cholesterol-related process and differ in many aspects of screening conditions, which generally results in poor consensus for the gene hits between different reports. These findings suggest that many more functional genes underlying cholesterol or lipid homeostasis need to be discovered with orthogonal or complementary screening approaches.

In the present study, we adopted a comprehensive multi-omics approach by combinatorial application of CRISPR screening, RNA sequencing, human genetic variant association analysis, and proteomic and metabolomic profiling techniques to catalog the genes related to cholesterol and lipid metabolism. We further characterize a top hit *GGT7*, encoding a gamma-glutamyltransferase, for its function and mechanism during cholesterol and lipid homeostasis using both cellular and genetic mouse models. These results provide both valuable datasets and critical insights into cholesterol and lipid metabolism.

Results

Genome-scale CRISPR screens identify key genetic interactions (GIs) underlying cholesterol homeostasis

Cholesterol is an essential molecule for cell survival and intracellular cholesterol is largely supplied via de novo biosynthesis and direct uptake from outside. Based on this fact, we surmise that the two key regulators of cholesterol biosynthesis and uptake, *HMGCR* and *LDLR*, respectively, should have a synthetic lethal interaction. Using independent single guide RNAs (sgRNAs), we successfully knocked out either *HMGCR* or *LDLR* in hepatic HepG2 cells (Fig. 1A and B). As expected, we did observe a dramatic loss of cell viability when the two genes were simultaneously perturbed compared to

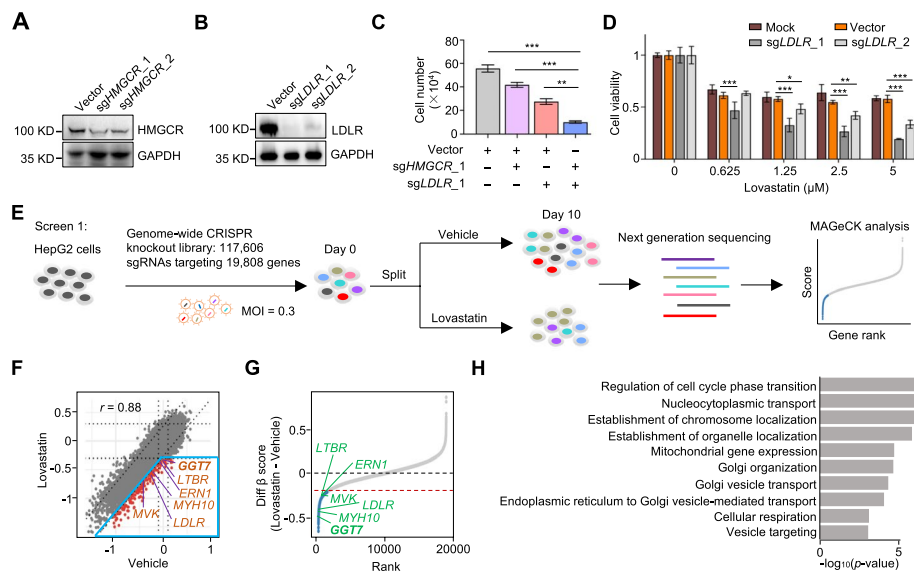


Fig. 1 Synthetic lethal CRISPR screening to identify potential cholesterol regulators in HepG2 cells. **A** Immunoblot analysis of HMGCR in HepG2 cells undergoing CRISPR-mediated gene knockout with two independent sgRNAs (numbered as _1 and _2). Vector without specific sgRNA insert serves as a control. GAPDH serves as a loading control. **B** Immunoblot analysis of LDLR in HepG2 cells that have undergone CRISPR-mediated gene knockout with two independent sgRNAs. **C** The cell growth analysis of HepG2 cells after introducing indicated sgRNAs via lentiviral infection for 7 days. Cells were counted with a hemacytometer. Mean \pm SD with $n = 3$. Ordinary one-way ANOVA with Tukey's test, ** $p < 0.01$, *** $p < 0.001$. **D** The relative cell viability was determined by CCK-8 assay for HepG2 cells expressing indicated sgRNAs and treated with indicated doses of lovastatin. Mean \pm SD with $n = 6$. Ordinary one-way ANOVA with Dunnett's test, * $p < 0.05$, ** $p < 0.01$, *** $p < 0.001$. **E** The workflow of genome-scale synthetic lethal CRISPR screens (Screen 1) to identify negative GIs with *HMGCR* using its inhibitor lovastatin in HepG2 cells. **F** The scatter plot showing the β score of each gene and the correlation of both CRISPR screens (vehicle and lovastatin) in HepG2 cells. The genes in blue box are preferential targets as the synthetic lethal or negative GI hits. **G** The rank-ordered list of each gene in the CRISPR screens according to the strength of synthetic lethality measured by differential β scores between lovastatin and vehicle conditions. The top interesting gene hits are highlighted. **H** The top selected functional terms enriched among synthetic lethal hits of the CRISPR screens (Screen 1) as determined by the gene ontology (GO) and Kyoto Encyclopedia of Genes and Genomes (KEGG) analysis

vector control or single gene knockout (KO) (Fig. 1C). Moreover, such synthetic lethality was also confirmed with lovastatin, a clinically used inhibitor of HMGCR, in *LDLR* KO cells (Fig. 1D).

Based on the above findings, we designed multiple cell viability-based synthetic lethal CRISPR screens in order to identify genetic interactions for key cholesterol regulators or pathways. For Screen 1, we used lovastatin to block the cholesterol biosynthesis pathway or the action of HMGCR, and tried to identify the genes whose loss-of-function were synthetic lethal with lovastatin in HepG2 cells using a genome-scale CRISPR KO screen (Fig. 1E). A β -score was assigned for each gene using MAGeCK algorithm to illuminate the phenotypic strength upon perturbation [29]. A negative score means decreased viability and a positive score represents increased cell fitness. The core essential genes underwent significantly negative selection in both vehicle and lovastatin conditions (Additional file 1: Fig. S1A and B) as expected, and the two samples generally correlated quite well ($r = 0.88$; Fig. 1F), further supporting the high quality of this screen. Using an arbitrary cutoff ($\text{score}_{\text{lovastatin}} - \text{score}_{\text{vehicle}} \leq -0.2$ and $\text{score}_{\text{lovastatin}} \leq -0.3$), we identified 368 genes as the synthetic lethal or negative GI hits for lovastatin or *HMGCR*

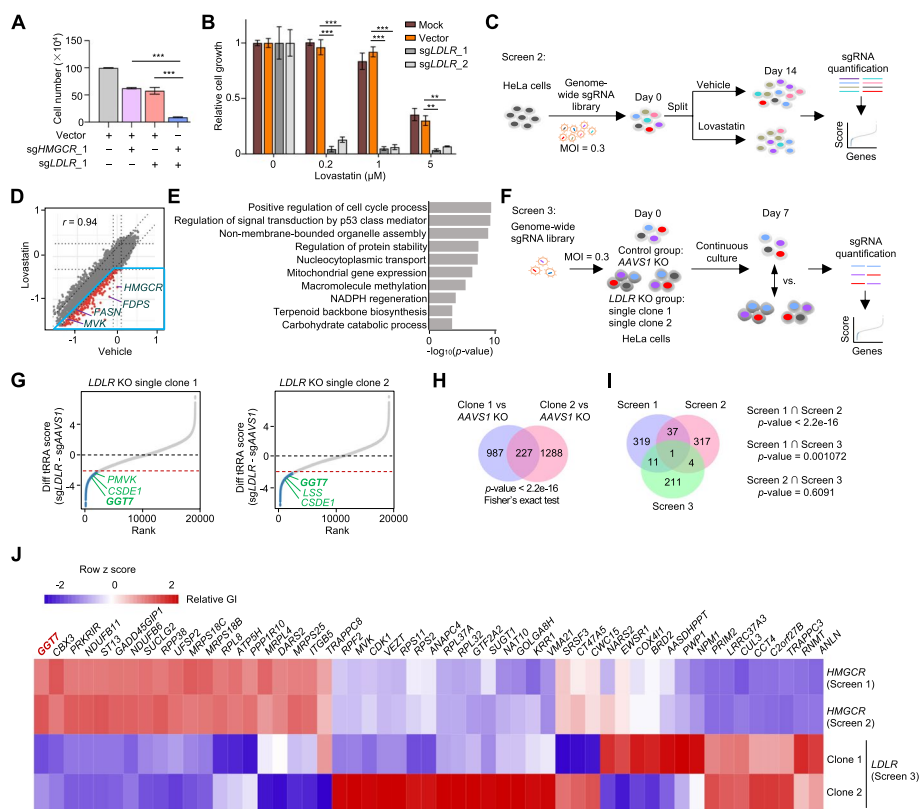


Fig. 2 Multiple CRISPR screens in HeLa cells for cholesterol regulatory genes. **A** The cell growth analysis of HeLa cells after introducing indicated sgRNAs via lentiviral infection for 7 days. Cells were counted with a hemacytometer. Mean \pm SD with $n = 3$. Ordinary one-way ANOVA with Tukey’s test, $***p < 0.001$. **B** The relative cell growth determined by cell counting for HeLa cells introducing indicated sgRNAs and treated with indicated doses of lovastatin. Mean \pm SD with $n = 3$. Ordinary one-way ANOVA with Dunnett’s test, $**p < 0.01$, $***p < 0.001$. **C** The workflow of genome-scale synthetic lethal CRISPR screens (Screen 2) to identify negative GIs with *HMGCR* using its inhibitor lovastatin in HeLa cells. **D** The scatter plot showing the β score of each gene and the correlation of both CRISPR screens (vehicle and lovastatin) in HeLa cells. The genes in blue box are preferential targets as the synthetic lethal or negative GI hits. **E** The top selected functional terms enriched among synthetic lethal hits of the CRISPR screens (Screen 2) as determined by the GO and KEGG analysis. **F** The workflow of genome-scale synthetic lethal CRISPR screens (Screen 3) to identify negative GIs with *LDLR* in *LDLR* KO single clone and *AAVS1* KO control HeLa cells. **G** The rank-ordered list of each gene in the CRISPR screens (Screen 3) according to the strength of synthetic lethality measured by differential tRRA scores between *LDLR* KO single clone and *AAVS1* KO control HeLa cells. The top interesting gene hits are highlighted. **H** Venn diagram showing the overlap of synthetic lethal or negative GI hits between the two independent *LDLR* KO clones in the CRISPR screens (Screen 3). **I** Venn diagram showing the overlap of synthetic lethal or negative GI hits between the three CRISPR screens. **J** Heatmap showing the relative strength of GIs of top selected hits to *HMGCR* or *LDLR* across different CRISPR screens

, including known cholesterol regulators such as *LDLR*, *MVK*, and *LTBR* (Fig. 1F and G, Additional file 2: Table S1). These genes were functionally enriched in either core biological processes (e.g., ribosome biogenesis) or specific functions (e.g., nucleocytoplasmic transport, mitochondrial gene expression, vesicle targeting, and transport) (Fig. 1H, Additional file 1: Fig. S1C).

To determine the effects of cellular background on GI identification, we further employed non-hepatic cervical cancer-derived HeLa cells for investigation. The synthetic lethality between *LDLR* and *HMGCR* was reproduced by both genetic and pharmaceutical perturbations in HeLa cells (Fig. 2A and B). Following similar procedures in

Screen 1, we performed Screen 2 in HeLa cells to identify synthetic lethality hits with lovastatin treatment or negative GIs with *HMGCR* (Fig. 2C). The screens were also of high quality to identify correct cell fitness genes (Additional file 1: Fig. S2A and B). Using similar criteria as Screen 1 ($\text{score}^{\text{lovastatin}} - \text{score}^{\text{vehicle}} \leq -0.2$ and $\text{score}^{\text{lovastatin}} \leq -0.3$) to identify synthetic lethal or negative GI hits for lovastatin or *HMGCR*, a total of 359 such hits were identified in HeLa cells (Additional file 2: Table S1). Interestingly, we found several genes responsible for cholesterol or lipid biosyntheses such as *HMGCR* itself, *MVK*, *FDPS*, and *FASN*, suggesting a high dependency on cholesterol or lipid biosynthesis for HeLa cells (Fig. 2D). In contrast, hepatic HepG2 cells seemed to depend on both biosynthesis pathway and LDLR-mediated uptake process to maintain proper intracellular cholesterol level (Fig. 1F and G). Functional gene enrichment analysis of these synthetic lethal hits showed that specific functional terms relating to p53 signaling and protein stability regulation were particularly enriched in HeLa cells (Fig. 2E), while other terms were also shared in HepG2 cells (Fig. 1H, Additional file 1: Fig. S2C and S1C), indicating a functional conserveness between different cell types.

Using two independent lines of *LDLR*-ablated single clonal HeLa cells (Additional file 1: Fig. S2D) and *AAVSI* KO cells as control, we further performed Screen 3 to determine negative GIs with *LDLR* (Fig. 2F, Additional file 1: Fig. S2E and F). A MAGeCK-derived tRRA score cutoff ($\text{score}^{\text{LDLR KO clone}} - \text{score}^{\text{AAVSI KO}} \leq -2$ and $\text{score}^{\text{LDLR KO clone}} \leq -1$) was employed to define synthetic lethal or negative GI hits for *LDLR*. Despite intrinsically clonal variations (e.g., different on-target sgRNAs, uncontrolled off-target editing, and clone-specific fluctuation), the two independent *LDLR* KO clones still produced a significant overlap of consensus synthetic lethal or negative GI hits (227) (Fig. 2G and H; Additional file 2: Table S1). Interestingly, mitochondria genes were significantly enriched among these consensus gene hits in Screen 3 (Additional file 1: Fig. S2G), further underscoring the functional interplay between mitochondria and lipid homeostasis [30, 31]. When comparing the results across the three CRISPR screens, we found a statistically significant overlap of synthetic lethal or negative GI hits for lovastatin or *HMGCR* between HepG2 (Screen 1) and HeLa (Screen 2) cells, suggesting the functional conserveness of those GIs across different cellular backgrounds (Fig. 2I). Meanwhile, none or less significant overlap was observed between negative GI hits for *LDLR* (Screen 3) and those for *HMGCR* (Screen 1 or 2) (Fig. 2I). Rather, an anti-correlative pattern of relative GIs with *LDLR* or *HMGCR* for shared gene hits of the three screens was observed (Fig. 2J). This is not only in agreement with the negative GI relationship between *LDLR* and *HMGCR* per se but also suggests a high quality and robustness of our results in pivotal GI identification underlying cholesterol homeostasis.

Notably, the cell fitness-based genetic screening systems do not exclusively rely on cholesterol restriction. Using untargeted metabolomic profiling, we found a dramatic decrease of multiple lipids including sterol lipids in *LDLR/HMGCR* double knock-out (DKO) HepG2 cells whereas single KO of *LDLR* or *HMGCR* had much less effect (Additional file 1: Fig. S3A–D, Additional file 3: Table S2). Therefore, the GIs identified here not only underlie cholesterol regulation but also contribute to broader and important lipid homeostasis.

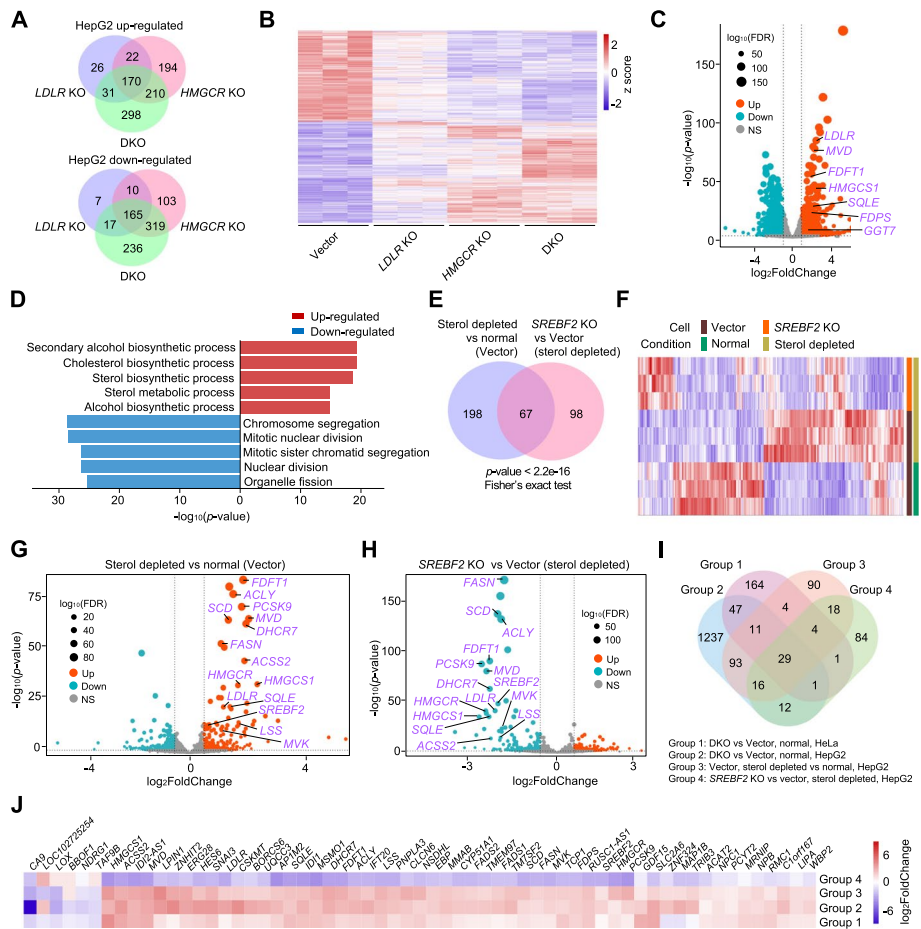


Fig. 3 Identification of potential cholesterol regulators at the transcriptional level. **A** Venn diagram showing the overlap of up- or down-regulated DEGs of HepG2 cells upon *LDLR* KO, *HMGCR*, or double KO (DKO) determined by RNA-seq analysis. **B** Heatmap showing the DEGs across different samples of HepG2 cells. **C** Volcano plot showing the DEGs in DKO cells compared to control HepG2 cells with several typical genes highlighted. **D** The top five enriched functional terms for either up-regulated or down-regulated DEGs in DKO cells compared to control HepG2 cells by GO and KEGG analysis. **E** Venn diagram showing the overlap of DEGs between sterol deprivation condition (sterol depleted vs. normal) and *SREBF2* KO under sterol deprivation (*SREBF2* KO vs. vector control) in HepG2 cells. **F** Heatmap showing the DEGs across indicated samples of HepG2 cells. **G** Volcano plot showing the DEGs between sterol deprivation and normal conditions of HepG2 cells with several representative genes highlighted. **H** Volcano plot showing the DEGs in *SREBF2* KO cells compared to vector control HepG2 cells in sterol deprivation condition with several representative genes highlighted. **I** Venn diagram showing the overlap of DEGs for indicated comparison groups. **J** Heatmap showing the expression change of representative DEGs that were shared between at least three comparison groups of **I**

Transcriptome profiling of cholesterol regulatory genes

As typical cholesterol regulator genes (e.g., *LDLR*, *HMGCR*, or *PCSK9*) often undergo feedback regulation in response to changes of intracellular cholesterol level, we tried to explore novel cholesterol regulatory genes by transcriptome profiling of genetically perturbed cells. First, we performed RNA sequencing (RNA-seq) in different HepG2 cells that were either depleted of *LDLR*, *HMGCR*, or both *LDLR/HMGCR*. Differentially expressed genes (DEGs) were identified for each group by comparison with control cells (Additional file 1: Fig. S4A, Additional file 4: Table S3). A great portion of genes were shared between the three genetically perturbed cells (Fig. 3A), highlighting their

consensus roles in maintaining cholesterol homeostasis. Interestingly, *HMGCR* KO cells are more assembled DKO cells than *LDLR* KO cells in terms of DEGs (Fig. 3B), suggesting that cholesterol biosynthesis is more pivotal than the uptake pathway in orchestrating intracellular cholesterol levels in HepG2 cells. Several known cholesterol regulators (e.g., *LDLR*, *MVD*, and *HMGCS1*) were present in the up-regulated genes upon *LDLR/HMGCR* DKO (Fig. 3C), again corroborating the feedback regulation during cholesterol homeostasis. The genes relating to cholesterol biosynthesis were more enriched in the up-regulated genes than in down-regulated genes in DKO cells (Fig. 3D), implying that we might identify novel cholesterol regulators from those up-regulated genes. Similar transcriptome profiling experiments were also performed using HeLa cells with similar conclusions (Additional file 1: Fig. S4B–F, Additional file 4: Table S3). The DEGs were largely shared between the three genetically perturbed HeLa cells (Additional file 1: Fig. S4C). Also, *HMGCR* KO was more alike to *LDLR/HMGCR* DKO than *LDLR* KO (Additional file 1: Fig. S4D), and up-regulated genes were more enriched for cholesterol-related processes (Additional file 1: Fig. S4E and F). Notably, the up-regulated DEGs were more significantly overlapped between HepG2 and HeLa cells than those down-regulated ones (Additional file 1: Fig. S4G), further supporting the functional conserveness of those up-regulated genes in orchestrating cholesterol homeostasis.

To further catalog potential cholesterol regulatory genes, we added another two groups of transcriptome comparison in HepG2 cells: one was to compare DEGs between sterol deprivation condition (DMEM supplemented with 10 μ M lovastatin without serum) and normal condition; and the other one was the comparison between *SREBF2* (encoding SREBP2, a key transcription factor for cholesterol regulatory genes) KO cells and vector control in sterol deprivation condition (Additional file 1: Fig. S4H, Additional file 4: Table S3). A significant portion of DEGs were shared between the two comparison groups (Fig. 3E) and a majority of up-regulated genes upon sterol deprivation were deregulated in *SREBF2* KO cells (Fig. 3F–H). Again, only those up-regulated genes in sterol starved condition and down-regulated genes upon *SREBF2* KO were enriched for cholesterol metabolism-related functional terms (Additional file 1: Fig. S4I and J). In addition, we highlighted those 29 genes that were reproducibly present in all four comparison groups (Fig. 3I and J), including several known key cholesterol regulators as well as several uncharacterized ones with potential cholesterol regulatory functions. Taken together, these data provided a repertoire of potential cholesterol regulators at the transcriptional level.

Integrative multi-omics analysis reveals GGT7 as a novel cholesterol regulator

To further explore candidate cholesterol regulators, we performed proteomics analysis to identify differential proteins in *LDLR/HMGCR* DKO HepG2 cells compared to those in control cells. Among 67 significantly up-regulated proteins, 48% of them were also present as DEGs in RNA-seq analysis (Fig. 4A and B, Additional file 5: Table S4). In contrast, the overlap for down-regulated proteins with DEGs in RNA-seq analysis was quite few (Fig. 4B), suggesting that more meaningful hits were present in up-regulated proteins or DEGs. Around 61% of differential proteins (55 out of 90) seemed to be regulated only at the proteinic level (Fig. 4B), necessitating the proteomics

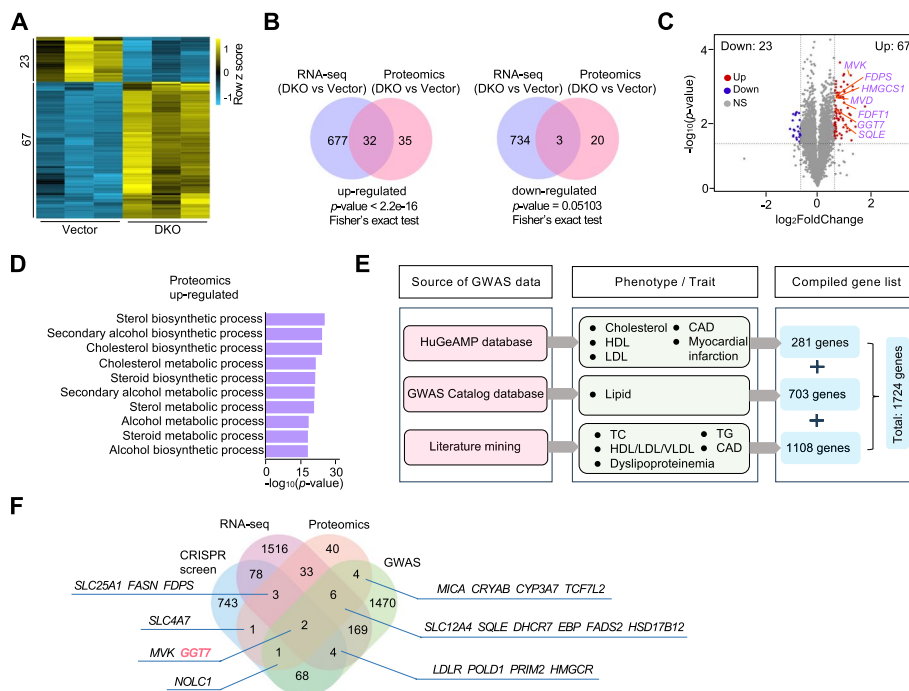


Fig. 4 Integrative multi-omics analysis to pinpoint key cholesterol regulators. **A** Heatmap showing the differentially expressed proteins in *LDLR/HMGCR* DKO cells compared to Vector control HepG2 cells determined by mass spectrometry-based proteomics profiling. The number of up- or down-regulated proteins is indicated along the heatmap. **B** Venn diagram showing the overlap of up-regulated or down-regulated genes in *LDLR/HMGCR* DKO cells compared to Vector control HepG2 cells between RNA-seq and proteomics analysis. **C** Volcano plot showing the differentially expressed proteins in *LDLR/HMGCR* DKO cells compared to control HepG2 cells with several typical proteins highlighted. **D** The top ten enriched functional terms for up-regulated proteins in *LDLR/HMGCR* DKO cells compared to control HepG2 cells by GO and KEGG analysis. **E** The analytic scheme of human genes associated with lipid disorders or cardiovascular diseases. HDL: high-density lipoprotein; LDL: low-density lipoprotein; VLDL: very low-density lipoprotein; TC: total cholesterol; TG: triglycerides; CAD: coronary artery disease. **F** Venn diagram showing the overlap of potential cholesterol or lipid regulators between different angles including synthetic lethal CRISPR screens (Screen 1–3), DEGs in RNA-seq analysis (DKO vs. vector in HepG2 and HeLa cells, sterol depleted vs normal, and *SREBF2* KO vs vector), differentially expressed proteins in proteomics analysis (DKO vs. vector in HepG2 cells), and the compiled list of human genes with variants related to lipid disorders or related diseases. The genes of indicated intersections are highlighted

analysis on top of RNA-seq experiments. Similarly, a cohort of pivotal cholesterol regulators was among the up-regulated differential proteins such as *MVK*, *MVD*, and *HMGCS1* (Fig. 4C), even using a more stringent cutoff (Additional file 1: Fig. S5A and B). Furthermore, only up-regulated differential proteins were significantly enriched for functional terms that were all related to sterol or cholesterol biosynthesis pathways (Fig. 4D, Additional file 1: Fig. S5C). To discover potential cholesterol regulators with human genetic evidence or clinical relevance, we explored public databases with Genome-Wide Association Study (GWAS) data and manually curated relevant literature to compile a gene list whose variants are associated with lipid-related traits or cardiovascular diseases (Fig. 4E, Additional file 6: Table S5). Next, we integrated data from CRISPR screens, RNA-seq, proteomics, and human genetic analysis for candidate cholesterol regulators (Fig. 4F). Apart from known genes, one gene named *GGT7*

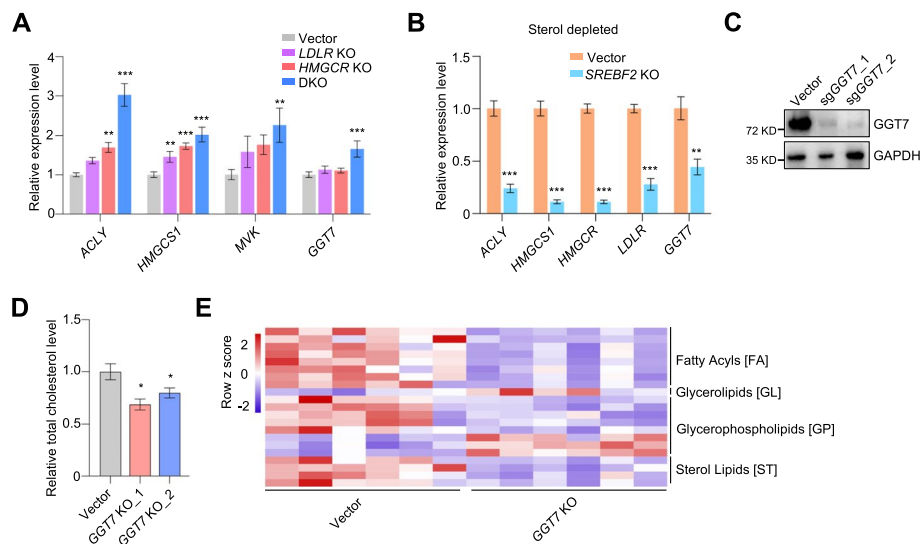


Fig. 5 Functions of *GGT7* during cholesterol and lipid homeostasis. **A** RNA expression analysis of indicated genes by RT-qPCR in HepG2 cells upon *LDLR* KO, *HMGCR* KO, or *LDLR/HMGCR* DKO. Mean \pm SD with $n = 3$. Ordinary one-way ANOVA with Dunnett's test, compared to Vector control, $**p < 0.01$, $***p < 0.001$. **B** RNA expression analysis of indicated genes by RT-qPCR in HepG2 cells upon *SREBF2* KO under sterol deprivation condition. Mean \pm SD with $n = 3$. Unpaired two-sided *t* test, compared to vector control, $**p < 0.01$, $***p < 0.001$. **C** Immunoblot analysis of *GGT7* in HepG2 cells undergoing CRISPR-mediated gene knockout with two independent sgRNAs. GAPDH serves as a loading control. **D** Decreased total cholesterol levels of HepG2 cells upon *GGT7* KO using two independent sgRNAs. Mean \pm SD with $n = 3$. Unpaired two-sided *t* test, compared to vector control, $*p < 0.05$. **E** Decreased sterol and other lipids upon *GGT7* KO in HepG2 cells determined by untargeted metabolomic profiling. $n = 6$ biological replicates for each group

caught our attention as it was present in all four categories and previously unrecognized to be implicated in cholesterol or lipid regulation.

GGT7 controls cholesterol and lipid metabolism

GGT7 encodes a γ -glutamyltransferase that is involved in glutathione metabolism and transpeptidation of amino acids. The γ -glutamyltransferases (GGTs) are mainly found in the liver and their increased activities in the blood often inform damaged functions of the liver or bile duct [32]. Our integrative analysis indicated that *GGT7* was functionally synthetic lethal with lovastatin or *LDLR* KO and up-regulated at both transcriptional and proteinic levels upon *LDLR/HMGCR* DKO (Figs. 1G, 2G, 3C, 4C, and F). Moreover, it was reported that the variants of *GGT7* are clinically associated with hypertension and type 2 diabetes in Chinese and Russian populations, respectively [33, 34]. Several clinical studies indicated a positive correlation between GGT activity and multiple metabolic characteristics including body mass index, blood pressure, total cholesterol, LDL-C, triglycerides (TG), and glucose [35], suggesting GGT as a novel biomarker for cardiovascular disease risk. These data imply that *GGT7* might be an important regulator underlying cholesterol or lipid homeostasis. Using reverse transcription quantitative PCR (RT-qPCR), we confirmed that *GGT7* mRNA, as other tested cholesterol regulatory genes, was significantly increased upon *LDLR/HMGCR* DKO (Fig. 5A). Furthermore, the expression of *GGT7* was significantly compromised in *SREBF2* KO cells under sterol deprivation condition (Fig. 5B), suggesting that *GGT7* was a SREBP2-dependent target.

To determine the functions of *GGT7* on cholesterol regulation, we knocked out *GGT7* using two independent sgRNAs in HepG2 cells (Fig. 5C) and measured total cholesterol levels of the cells. As shown in Fig. 5D, *GGT7* knockout significantly decreased cellular cholesterol levels, indicating that *GGT7* was indeed a cholesterol regulator. Moreover, untargeted metabolomic analysis showed that, in addition to sterol lipids, the levels of several other lipids such as fatty acyls were also deregulated upon *GGT7* knockout in HepG2 cells (Fig. 5E, Additional file 1: Fig. S5D, Additional file 3: Table S2). These results indicate that *GGT7* is a pivotal regulator for cholesterol and lipid metabolism.

The mechanistic insights of *GGT7* in cholesterol regulation

To determine how *GGT7* orchestrates cholesterol homeostasis, we firstly examined the expression of typical cholesterol regulators upon *GGT7* knockout in HepG2 cells. A large portion of tested genes were affected, further supporting the pivotal roles of *GGT7* in cholesterol homeostasis (Fig. 6A). Notably, most of them were regulated in a direction towards a feedback response to cholesterol insufficiency. For example, the genes accounting for cholesterol biosynthesis and SREBP2 pathway (e.g., *ACLY*, *HMGCS1*, and *MBTPS2*) were increased, while the negative regulators mediating cholesterol transport and storage (e.g., *PCSK9* and *PLIN2*) were decreased (Fig. 6A). When cells were cultured in sterol deprivation condition, *LDLR*, *HMGCR* and *SREBF2* were also significantly increased to complement the insufficiency of intracellular cholesterol in *GGT7*-deficient cells (Fig. 6B). On the other hand, we did observe some genes that were deregulated to cause decreased cellular cholesterol upon *GGT7* knockout. For instance, *SORL1*, which was reported to mediate cholesterol uptake into neuronal cells by acting as a receptor for apolipoprotein E [36], was significantly down-regulated and might play a causal role in cholesterol insufficiency in *GGT7*-ablated cells (Fig. 6A). To obtain a complete view of *GGT7* downstream target genes, we performed RNA-seq experiments to profile DEGs in *GGT7* KO HepG2 cells (Additional file 4: Table S3). Compared to the control group, more genes were down-regulated rather than up-regulated (Fig. 6C), and those cholesterol regulators tested in RT-qPCR displayed similar trends in RNA-seq data (Fig. 6A–C). Top enriched functional terms included “glycolysis,” “lipid or cholesterol transport,” and “cholesterol metabolic process” (Fig. 6D), further confirming the important functions of *GGT7* in cholesterol homeostasis.

To further reveal the working mechanism of *GGT7*, we exogenously expressed *GGT7* in HepG2 cells and employed immunoprecipitation coupled with mass spectrometry to identify its associated protein partners (Fig. 6E and F, Additional file 1: Fig. S6A and B). The top interacting candidate was a myosin protein MYH10 (Myosin-10) which belongs to a large family of actin-based cytoskeletal motors responsible for cargo or vesicle transport (Fig. 6F). We validated the endogenous interaction between *GGT7* and MYH10 using immunoprecipitation coupled with immunoblot analysis in HepG2 cells (Fig. 6G). To determine the functional effect of *MYH10* during cholesterol homeostasis, we knocked out *MYH10* in HepG2 cells (Fig. 6H) and found a significant decrease of cellular cholesterol which phenocopied *GGT7* knockout (Fig. 6I). Furthermore, similar to *GGT7*, *MYH10* was also identified as a synthetic lethal hit or negative GI with lovastatin or *HMGCR* in our functional CRISPR screens (Fig. 1F and G). Considering that “cholesterol transport” was enriched among *GGT7* downstream targets (Fig. 6D)

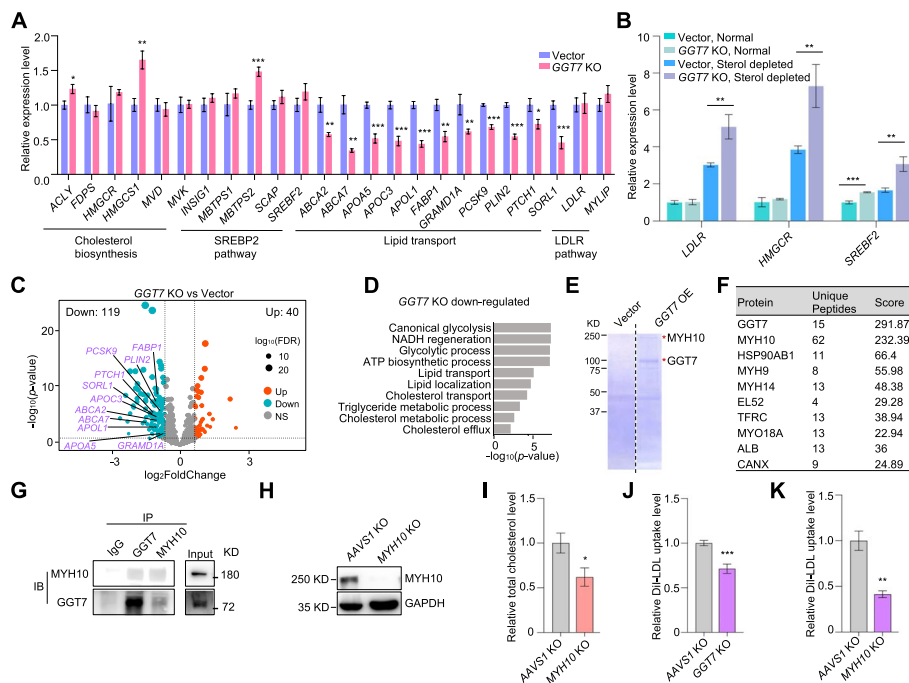


Fig. 6 Mechanistic insights of *GGT7* in regulating cholesterol metabolism. **A** RNA expression analysis of indicated genes by RT-qPCR in HepG2 cells upon *GGT7* KO. Mean \pm SD with $n = 3$. Unpaired two-sided t test, compared to Vector control, * $p < 0.05$, ** $p < 0.01$, *** $p < 0.001$. **B** RNA expression analysis of indicated genes by RT-qPCR in HepG2 cells upon *GGT7* KO under normal or sterol deprivation conditions. Mean \pm SD with $n = 3$. Unpaired two-sided t test, * $p < 0.05$, ** $p < 0.01$, *** $p < 0.001$. **C** Volcano plot showing the DEGs in *GGT7* KO cells compared to vector control HepG2 cells with several typical genes highlighted. The number of up- or down-regulated DEGs is indicated. **D** The top selected functional terms enriched for down-regulated DEGs in *GGT7* KO cells compared to control HepG2 cells by GO and KEGG analysis. **E** Coomassie blue staining of SDS-PAGE gel with FLAG bead immunoprecipitated materials from vector control- or FLAG-*GGT7*-expressing HepG2 cells. The band position corresponding to *GGT7* or *MYH10* is indicated with an asterisk. **F** The top ten list of *GGT7*-interacting protein partners identified by mass spectrometry. **G** Immunoblot analysis of total cell lysis and immunoprecipitants (using IgG control, *GGT7*, or *MYH10* antibody) for indicated proteins derived from HepG2 cells. **H** Immunoblot analysis of *MYH10* in HepG2 cells that have undergone CRISPR-mediated gene knockout. GAPDH serves as a loading control. **I** Decreased total cholesterol levels of HepG2 cells upon *MYH10* knockout. Mean \pm SD with $n = 3$. Unpaired two-sided t test, compared to *AAVS1* KO, * $p < 0.05$. Decreased Dil-LDL uptake by HepG2 cells upon **J** *GGT7* or **K** *MYH10* knockout. Mean \pm SD with $n = 3$. Unpaired two-sided t test, compared to *AAVS1* KO, ** $p < 0.01$, *** $p < 0.001$

and the involvement of other myosins or cytoskeleton-associated proteins during LDL transport such as Myosin Vb and LIMA1 [10], we speculated that *GGT7* might work together with *MYH10* to regulate cholesterol or LDL-C uptake. Indeed, knockout of either *GGT7* or *MYH10* consistently led to a decrease of fluorophore-labeled Dil-LDL uptake (Fig. 6J and K), suggesting that *GGT7*'s action on cholesterol homeostasis can be partially through *MYH10*-involved cholesterol uptake. Meanwhile, the regulatory functions of *GGT7* on biomolecule metabolism might also play a role in orchestrating cellular cholesterol levels.

Ggt7^{-/-} mice display impaired cholesterol and lipid homeostasis

To explore the in vivo functions of *GGT7* on cholesterol homeostasis, we decided to construct a genetically modified mouse model for its mouse homolog *Gtg7*. We first analyzed the expression patterns of *GGT7* or *Gtg7* across various human and mouse tissues

using RNA-seq data from a public database and found a dramatic difference between human and mouse (Additional file 1: Fig. S7A and B). *GGT7* was broadly expressed in many human tissue types with brain tissue showing the highest expression. In contrast, mouse *Ggt7* seemed to be exclusively expressed in brain tissue (Additional file 1: Fig. S7A and B). Using RT-qPCR, we confirmed that *Ggt7* was indeed quite highly expressed in mouse brain tissue followed by the spinal cord and testis while other tissues barely expressed it (Additional file 1: Fig. S7C). Such tissue specificity discordance somehow hindered faithful evaluation of human *GGT7* in mouse models and might be explained by various expression patterns and cross activities of other GGT family members.

As *GGT7* in general was not an essential gene according to the DepMap database (Additional file 1: Fig. S7D), we continued to establish a whole-body *Ggt7* knockout mouse model by CRISPR-based method to evaluate its in vivo functions (Fig. 7A and B, Additional file 1: S7E and F). As expected, *Ggt7*^{-/-} mice were viable and followed normal Mendelian ratios. We then challenged them with a high fat/high cholesterol (HFHC) diet and evaluated the effect of *Ggt7* ablation on lipid metabolism. HFHC diet caused an increase of body weight for both *Ggt7*^{+/+} and *Ggt7*^{-/-} mice compared to those fed under a normal diet (ND) (Fig. 7C). Interestingly, *Ggt7*^{-/-} mice displayed a significantly lower body weight for the ND group and similar trend still held for HFHC group though not statistically significant (Fig. 7C). The circulating total cholesterol levels in the blood were significantly decreased in *GGT7*^{-/-} mice especially under HFHC diet (Fig. 7D). Similar trend was also observed for the blood high-density lipoprotein cholesterol (HDL-C) level, while the decrease of circulating LDL-C was mainly evident in *Ggt7*-ablated mice fed with ND (Fig. 7E and F). In contrast, we did not observe an apparent difference in TG in the blood between *Ggt7*^{+/+} and *Ggt7*^{-/-} mice (Fig. 7G). Furthermore, the liver size and functions as evidenced by serum alanine transaminase (ALT) and aspartate transaminase (AST) assays were not significantly changed upon *Ggt7* KO (Additional file 1: Fig. S7G–I). Unlike in humans, serum GGT in mice or rats is usually very low or even undetectable according to previous studies [37]. Consistently, we failed to detect serum GGT activity using a commercial detection kit in both *Ggt7*^{+/+} and *Ggt7*^{-/-} mice. Although the lipid droplet was more accumulated in liver tissue under the HFHC diet compared to ND, no significant difference was observed between *Ggt7*^{+/+} and *Ggt7*^{-/-} mice (Additional file 1: Fig. S7J). Concordantly, the levels of total cholesterol and TG in the livers were neither changed in *Ggt7*-ablated mice (Fig. 7H and I). This was consistent with the notion that *Ggt7* expression is low in mouse liver. However, in mouse brain tissue where *Ggt7* is highly expressed, we did see a minor decrease in total cholesterol and a significant drop in TG levels in *Ggt7*^{-/-} mice under either ND or HFHC diet (Fig. 7J and K). These data demonstrate that *Ggt7* plays an important role in cholesterol and lipid homeostasis in mice. We further collected tissue samples of mouse brain or liver for RNA-seq analysis ($n=5$ for each group), and DEGs were identified by comparison between *Ggt7*^{+/+} and *Ggt7*^{-/-} groups (Additional file 4: Table S3). We found more DEGs in the brain than those in the liver (Fig. 7L). Although the overlap of DEGs between the two tissue types was low (Fig. 7M), those DEGs seemed to be functionally important for either the brain or liver as evidenced by gene enrichment analysis (Fig. 7N). Whole-body KO of mouse *Ggt7* affected genes related to “neural development and functional processes” in the brain, whereas, in the liver, the deregulated genes were preferentially

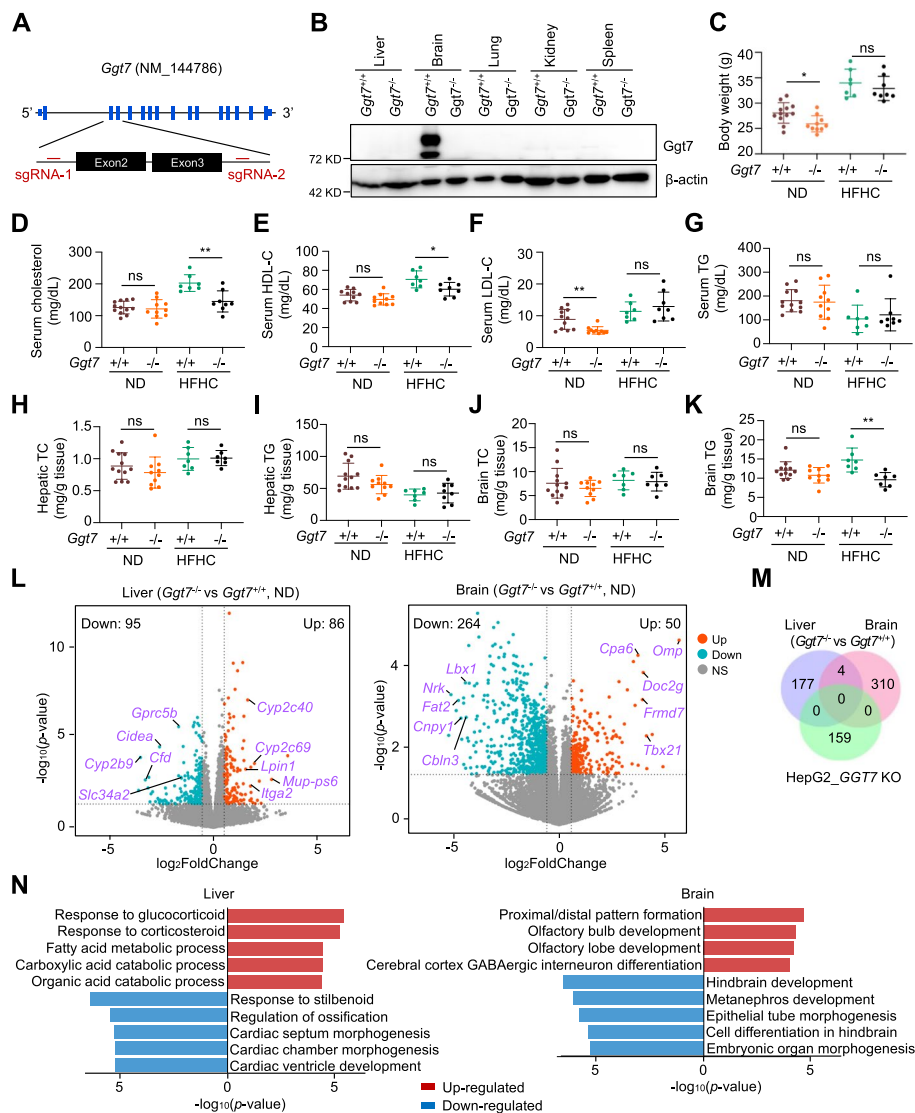


Fig. 7 Impaired cholesterol and lipid homeostasis in *Ggt7* knockout mice. **A** The construction strategy of whole-body *Ggt7* KO mice using two sgRNAs targeting the flanks of exon 2 and exon 3 of *Ggt7* in the mouse genome. **B** Immunoblot analysis of *Ggt7* in different types of tissues derived from *Ggt7*^{+/+} and *Ggt7*^{-/-} mice. β -actin serves as a loading control. **C** Body weight measurements for *Ggt7*^{+/+} and *Ggt7*^{-/-} mice under normal diet (ND) ($n = 12$ and 10, respectively) or high-fat high cholesterol (HFHC) diet ($n = 7$ and 8, respectively). Unpaired two-sided t test, $*p < 0.05$, ns means not significant. **D** The serum total cholesterol levels ($n = 12, 10, 7$ and 8 for each group), **E** serum HDL-cholesterol (HDL-C) levels ($n = 10, 10, 7$ and 8), **F** serum LDL-cholesterol (LDL-C) levels ($n = 11, 10, 7$ and 8) and **G** serum triglycerides (TG) levels ($n = 12, 10, 7$ and 8) in *Ggt7*^{+/+} and *Ggt7*^{-/-} mice fed with ND or HFHC diet. Unpaired two-sided t test, $*p < 0.05$, $**p < 0.01$, ns means not significant. **H** The total cholesterol (TC) levels ($n = 12, 10, 7$ and 7) or **I** TG levels ($n = 12, 10, 7$ and 8) in the livers of *Ggt7*^{+/+} or *Ggt7*^{-/-} mice fed with ND or HFHC diet. Unpaired two-sided t test, ns means not significant. **J** The TC levels ($n = 12, 10, 7$, and 7) or **K** TG levels ($n = 12, 10, 7$, and 7) in the brain tissues of *Ggt7*^{+/+} or *Ggt7*^{-/-} mice fed with ND or HFHC diet. Unpaired two-sided t test, $**p < 0.01$, ns means not significant. **L** Volcano plot showing the DEGs upon *Ggt7* knockout in the mouse liver or brain tissues. The number of up- or down-regulated DEGs is indicated. **M** Venn diagram showing the overlap of DEGs between *Ggt7* KO in mouse liver, *Ggt7* KO in mouse brain, and *GGT7* KO in HepG2 cells as determined by RNA-seq analysis. **N** The top five enriched functional terms for either up-regulated or down-regulated DEGs in the liver or brain tissues of *Ggt7*^{-/-} mice vs. *Ggt7*^{+/+} mice

implicated in liver functions such as “response to hormones” or “biomolecule metabolic processes” (Fig. 7N). Notably, the overlap of DEGs between mouse tissues and human HepG2 cells upon *GGT7* KO was also not significant (Fig. 7M), further suggesting a functional difference between different species as well as in vivo versus in vitro systems. Nevertheless, these results corroborate that *GGT7* can orchestrate cholesterol and lipid homeostasis in vivo.

Discussion

Unraveling the cholesterol regulatory genes is important for understanding the molecular basis of cholesterol and lipid metabolism and for developing novel therapeutics against related diseases. In this study, we integrated multiple high-throughput approaches from functional genetics to multi-omics profiling and systematically cataloged cholesterol regulatory genes at genetic, transcriptional, proteomic, and functional levels. These datasets and gene repertoire offered valuable resources to the relevant research fields. In addition, we further validated a gamma-glutamyltransferase *GGT7* as a novel regulator for cholesterol and lipid metabolism in both cell line models and genetically modified mice. This work functionally linked a well-established liver damage indicator to cholesterol and lipid homeostasis, suggesting the possibility of using gamma-glutamyltransferase as both a diagnostic biomarker and therapeutic target for cardiovascular diseases.

Pioneering researchers have elucidated the core signaling and cellular pathways relating to cholesterol biosynthesis, uptake and export, trafficking, and esterification [2]. However, the key functional genes accounting for these processes identified to date are still limited. Our integrative multi-omics approaches here leveraged both the power of functional genomics and the comprehensiveness of large omics profiling. The gene landscape we described here not only contains the cholesterol-responsive or -regulatory genes across different cell types at transcriptional or translational levels but also manifests the complicated genetic interactions between those functional genes. In addition to those known cholesterol-related genes, we were able to identify many more intriguing hits that were worthy of further investigation in future studies.

Multiple layers of evidence ranging from CRISPR screening to transcriptional and proteomic profiling pointed to *GGT7* as a novel regulator of cholesterol and lipid homeostasis. We demonstrated that loss-of-function of *GGT7* down-regulated intracellular cholesterol levels in cells and serum cholesterol levels in mice. As an uncharacterized gamma-glutamyltransferase, *GGT7* is evolutionarily divergent to classic gamma-glutamyltransferase *GGT1* [32], suggesting that additional functions of *GGT7* may exist. *GGT7* is down-regulated in glioblastoma and gastric cancer, and functions as a tumor suppressor possibly via its regulation of glutathione metabolism and associated redox status [38, 39]. Interestingly, in *GGT7*-overexpressing gastric cancer cells, the most significantly enriched functional term for differentially expressed genes is “steroid biosynthesis” [39]. Moreover, Rab7 was identified as one of the most prominent *GGT7*-interacting proteins in gastric cancer cells [39]. Another recent study showed that Rab7 GTPase controls NPC1-dependent lysosomal cholesterol export [26]. These findings agree with our results that *GGT7* may fulfill its function by regulating cholesterol metabolism. Although the enzymatic activity test of gamma-glutamyltransferase

has been introduced for several decades as an indicator of liver damage, the knowledge about the genes encoding these GGT enzymes remains quite limited. Clinical observations from several cross-sectional and longitudinal studies showed that increasing GGT levels were positively correlated with body mass index, total cholesterol, LDL-C, and the risk of all-cause mortality [33, 35, 40–48], suggesting GGT level as an independent or stand-alone risk factor for cardiovascular diseases. Here, we provide the first evidence, to our knowledge, in basic biology that GGT enzymes directly participate in the control of cholesterol levels. By establishing such a causal link between GGT7 and cholesterol levels, our work not only corroborates the validity of using GGT level as a biomarker of cardiovascular diseases but also suggests a potential way of therapeutic interventions by targeting GGT7 via inhibitory compounds or monoclonal antibodies. Before moving forward, it is still necessary to elucidate the molecular mechanism of GGT7 and the contribution of other GGT family enzymes to cholesterol homeostasis.

There are several limitations to the current study. First, the functional CRISPR screens here depended on cell fitness as the readout, which phenotype could be affected by many factors and was not exclusively due to cholesterol or lipid insufficiency. Therefore, the results must be interpreted together with other evidence to specifically claim cholesterol regulatory genes. Second, our interrogation of potential cholesterol regulators was mainly performed in limited cell models especially human hepatoma HepG2 or cervical cancer HeLa cells. More cell models of different tissue types and non-cancerous origin are needed in future work to expand the functional gene list and to correct the bias from individual cell models. Third, due to the expression and functional discrepancies between human and mouse species, the genetic mouse model of *Ggt7* would not faithfully reflect the *in vivo* function of the human *GGT7* gene. In addition, the potentially functional redundancy and crosstalk between multiple members of gamma-glutamyltransferases further added complexity to this issue. Finally, as an initial effort to systematically screen potential cholesterol and lipid regulators, we did not put much emphasis on elucidating the detailed molecular mechanisms of any single hit even for *GGT7*. Future work is needed to carefully explore the potential interplay between gamma-glutamyltransferases and cholesterol homeostasis especially in the context of cardiovascular diseases.

Conclusions

In summary, our study comprehensively maps cholesterol or lipid-related genes using an integrative multi-omics approach and functionally connects a gamma-glutamyltransferase gene *GGT7* to cholesterol and lipid homeostasis. Further work is needed to decipher the detailed molecular mechanism of *GGT7* in orchestrating cholesterol metabolism and to explore the possibility of targeting gamma-glutamyltransferase for treating cardiovascular diseases.

Methods

Cell line models

Human hepatic cancer cell line HepG2, cervix cancer cell line HeLa, and HEK293FT cells were obtained from the American Type Culture Collection (ATCC). Authentication was not performed after obtaining these cells. All the cells were maintained in Dulbecco's

modified Eagle's medium (DMEM) with 10% fetal bovine serum (FBS, Notacor) and 1% penicillin/streptomycin (Gibco). Sterol deprivation medium was DMEM supplemented with 10 μ M lovastatin without FBS. Cells were cultured in a 5% CO₂ atmosphere at 37 °C. All the cell lines were tested negative for mycoplasma.

Mouse models

All animal care and experimental procedures used in this study were approved by the Animal Care and Use Committee of Northeastern University (NEU-EC-2021A019S), according to national and institutional guidelines. Mice were housed under a 12-h light–dark cycle with free access to water and a normal chow diet supplemented with 20% crude protein (Beijing Huafukang Bioscience, 1022), except as noted. All mice used were bred on the C57BL/6 J background. *Ggt7* whole-body knockout mice were generated by using a CRISPR/Cas9-based protocol. Briefly, Cas9 mRNA, sgRNAs, and donor plasmids were injected into fertilized zygotes. Sequences of sgRNAs and donor oligos used for generating *Ggt7* whole-body knockout mice are shown in Additional file 7: Table S6. The microinjection and initial breeding were performed by Cyagen company. Founder \pm *Ggt7*^{+/-} mice were bred with C57BL/6J for two rounds. *Ggt7*^{+/+} and *Ggt7*^{-/-} littermates were generated by breeding *Ggt7*^{+/-} mice. For studies with special diets, 15-week-old male mice were placed on high-fat/high-cholesterol diet (normal diet plus 1.25% cholesterol, 15% fat, and 0.5% cholic acid, Beijing Huafukang Bioscience) for a total period of 30 weeks. Body weight was recorded at the endpoint of the treatment period. Blood samples were clotted at room temperature for 30 min followed by centrifugation at 3000 rpm for 10 min at 4 °C. The supernatant was collected and stored at –80 °C until use. Mice were anesthetized using isoflurane (RWD Life Science).

Plasmid construction

The sgRNAs were cloned into pLentiCRISPRv2-Puro (Addgene, 52961) using the *BsmBI* restriction enzyme site. The sgRNA sequences are listed in Additional file 7: Table S6. The expression construct for FLAG-tagged GGT7 was generated via Gibson assembly using the linearized pHAGE-EF1 α -puro lentivector and RT-PCR amplified *GGT7* cDNA (NM_178026) fragment (with a N-terminal FLAG sequence and a C-terminal HA sequence) from HepG2 cells.

Lentivirus production and transduction

Lentiviruses were packaged in HEK293FT cells. Cells were transfected the following day after seeding, with a lentiviral expression vector, the packaging vectors pCMV R8.74 and pMD2.G at a ratio of 1:0.75:0.5 using Lipofectamine 2000 transfection reagent (Thermo Fisher Scientific, 11668030). Six hours post transfection, the media were replaced with fresh media. Supernatants containing the secreted lentiviruses were collected twice at 48 h and 72 h followed by centrifugation at 3000 rpm for 5 min to remove the cellular debris. The collected lentiviruses were stored at –80 °C before use. For lentiviral transduction of target cells (HepG2 and HeLa), lentiviruses were directly added to the cell culture media with 6 μ g/mL polybrene. To get rid of uninfected cells, puromycin (Solarbio, P8230) selection (1.5 μ g/mL puromycin for 72 h) can be performed after 48 h post infection.

Cell growth and viability assay

HepG2 cells and HeLa cells were plated at 4×10^3 cells per well in DMEM with 10% FBS and 1% penicillin/streptomycin (normal medium) in 12-well plates. The cells were infected with lentiviruses expressing vector, sgRNAs targeting *LDLR* or *HMGCR*. The medium was changed every 2–3 days. The cell number was counted after 7 days with a hemacytometer. For detecting the synthetic lethal of lovastatin treatment in HeLa *LDLR* KO cells, cells were plated at 4×10^3 cells per well in the normal medium into 12-well plates. After incubation for 24 h, the cells were treated with lovastatin (Med-Chem Express, HY-N0504) with gradient concentrations. Seven days later, the cell number was counted with a hemacytometer and then normalized to the vehicle group. For detecting the synthetic lethal of lovastatin treatment in HepG2 *LDLR* KO cells, cells were plated at 1×10^3 cells per well in the normal medium into 96-well plates. After incubation for 24 h, the cells were treated with lovastatin with gradient concentrations. Seven days later, 10 μ L of CCK-8 reagent (Hanbio, HB-CCK-8–5) was added to each well. Following 1 h of incubation at 37 °C, the absorbance was recorded at 450 nm using the microplate reader (Gene Company Limited, Synergy H1).

Genome-wide CRISPR screening

The genome-wide CRISPR knockout screens were performed with a human H3 CRISPR knockout library (Addgene pooled library, 133914) which was designed with improved algorithms and superior performance. It consists of 117, 606 sgRNAs targeting more than 18,000 protein-coding genes in the human genome under the lentiviral pLentiCRISPRv2-Puro vector backbone. The plasmid library was amplified in electroporated *E. coli* electrocompetent cells with enough coverage and the plasmid pool was extracted using EndoFree Plasmid Maxiprep Kit (TianGen, DP117). To produce a lentivirus library, the plasmid pool was transfected into HEK293FT cells in 15 cm dishes along with those packaging plasmids. Transfection conditions were as follows: 20 μ g pLentiCRISPRv2-Puro, 15 μ g pCMV R8.74, 6 μ g pMD2.G, 80 μ L transfection reagent X-tremeGENE and 3 mL serum-free OPTI-MEM per plate. The medium was changed 16 h post-transfection. Lentiviral supernatants were collected, centrifuged, and stored at -80 °C before use. Around 1.2×10^8 HepG2 or HeLa cells were transduced at a low multiplicity of infection (MOI) of ~ 0.3 with the viral pool to achieve an average coverage of more than $300 \times$. Cells were treated with puromycin for 72 h and 3×10^7 cells were harvested as a sample of Day 0 (start point). The remaining cells were divided into two parts for the further vehicle or lovastatin treatment (0.3 μ M for HepG2 or 0.2 μ M for HeLa). At least 3×10^7 cells were maintained at any given time point to ensure enough sgRNA representation. Cells were passaged every 3 days. Treated HepG2 cells were harvested on Day 10 while HeLa cells were harvested on day 14 as endpoint. Genomic DNA (gDNA) was isolated from harvested cell samples via the classical isopropanol precipitation method. The sgRNA sequences were amplified from gDNA using a two-step nested PCR approach using the primer sequences listed in Additional file 7: Table S6. All PCRs were performed using Q5 High-Fidelity DNA Polymerase (New England Biolabs, M0491S). Illumina adaptors and barcodes were introduced via the last round of PCR to construct sequencing libraries. The final

PCR products were gel purified and pooled for PE150 high-throughput sequencing (Novogene) to determine the abundance of sgRNAs.

Analysis of CRISPR screening data

The MAGeCK algorithms were used for CRISPR screening analysis with default parameters [29]. The raw FASTQ files of sequencing data were processed and trimmed to retrieve sgRNA target sequences followed by the calculation of sgRNAs in the reference sgRNA library file using MAGeCKFlute [29]. For Screen 1 and Screen 2, the gene selection status was measured by a “ β score” generated by the MAGeCK-MLE function. A positive β score ($\beta > 0$) means the corresponding gene is enriched or positively selected after screening, whereas a negative β score ($\beta < 0$) indicates the corresponding gene is depleted or negatively selected. Synthetic lethal or negative GI hits in Screen 1 or Screen 2 were selected by β Score^{lovastatin} – Score^{vehicle} ≤ -0.2 and Score^{lovastatin} ≤ -0.3 . For Screen 3, a transformed RRA (tRRA) score generated via ReadRRA function through returning the log10 transformed RRA score was employed to indicate gene selection status during the screening by comparing sgRNA count at the end point of screen versus that of corresponding Day 0 for each sample. Synthetic lethal or negative GI hits in Screen 3 were selected by tRRA Score^{LDLR KO clone} – Score^{AAVSI KO} ≤ -2 and Score^{LDLR KO clone} ≤ -1 . Core essential genes are expected to be negatively selected in cell fitness screens. The list of core essential genes is provided by MAGeCKFlute [29]. The strength of negative GI was defined as differential values of β Score or tRRA Score between lovastatin treatment vs. vehicle or *LDLR* KO clone vs. *AAVSI* KO control samples.

Untargeted metabolomic profiling

HepG2 cells (1.5×10^6) were infected with lentiviruses to generate *LDLR* KO, *HMGCR* KO, or *LDLR/HMGCR* DKO HepG2 cells. After continuous culture for 6 days, cells were washed twice with pre-chilled PBS, and dissolved in 1 mL pre-chilled 60% methanol (Chromatographic grade). Cells were then centrifuged at 1000 g for 1 min at 4 °C to collect the pellet. The collected samples were further processed by Novogene company for LC–MS/MS analysis. LC–MS/MS analysis was performed on a Vanquish UHPLC system coupled to a Q-Exactive HF-X (Thermo Fisher Scientific) in both ESI positive and negative modes. LC–MS/MS data alignment, peak picking, adduct deconvolution, normalization, and identification were performed using Progenesis QI (Waters, Nonlinear Dynamics, UK) software. Lipid annotations were performed using KEGG, HMDB, and LIPID MAPS database. Six replicates were performed for each condition. Significantly changed metabolites were defined with the cutoff of $|\text{FoldChange}| \geq 2$, p -value ≤ 0.05 , and VIP (Variable Importance in Projection) ≥ 1 . A more stringent cutoff of $|\text{FoldChange}| \geq 2$, p -value ≤ 0.01 , and VIP ≥ 1 was also used. For untargeted metabolomic profiling of *GGT7* KO or vector control HepG2 cells, the samples were prepared following similar procedures as above, while LC–MS/MS analysis was different due to the upgrade of the instrument and software (Novogene). Briefly, LC–MS/MS data alignment, peak picking, and identification were performed using CD software. Lipid annotations were performed using Lipidblast and the LIPID MAPS database. Six replicates were performed for each condition. Significantly changed metabolites were defined with the cutoff of $|\text{FoldChange}| \geq 1.5$, p -value ≤ 0.05 , and VIP ≥ 1 . A more stringent cutoff of

$|\text{FoldChange}| \geq 1.5$, $p\text{-value} \leq 0.01$, and $\text{VIP} \geq 1$ was also used. The heatmap was plotted by the pheatmap R package.

RNA isolation and qPCR

Total RNA was isolated from cells using a UNIQ-10 Trizol total RNA extraction kit (Sangon, B511321). One microgram of total RNA was reverse transcribed using a High-Capacity cDNA Reverse Transcription Kit (Applied Biosystems, 4368814). Mouse tissues were weighed up to 50 mg, dissolved in Trizol reagent, lysed by homogenization and sonication. Lysates were clarified by centrifuging at 12,000 rpm for 5 min at 4 °C. The following RNA extraction and cDNA reverse transcription were similar to the procedures used for cells. The SYBR mixture (Cwbio, CW0957H) was used for qPCR performed on a QuantStudio™ 5 System (Applied Biosystems) with an initial 95 °C step for 10 min followed by 40 cycles of denaturation at 95 °C for 10 second (s), annealing at 60 °C for 30 s, and extension at 72 °C for 32 s. Gene expression levels were normalized to the expression level of internal control gene *RPS28* or *Rplp0* in human cells or mouse tissues, respectively. Each sample was analyzed in triplicate wells for qPCR. Relative mRNA levels were quantified using the $\Delta\Delta\text{Ct}$ method. Primer sequences are listed in Additional file 7: Table S6.

RNA-seq analysis

HepG2 or HeLa cells were cultured in a normal medium for 7 d, and then scraped in Trizol reagent. Mouse liver or brain tissues were collected and snap-frozen in liquid nitrogen before storage at -80 °C. Frozen liver or brain tissues (~ 20 mg) were homogenized and lysed in Trizol reagent. Total RNA was isolated as above. For samples of *SREBF2* KO vs. vector control and sterol deprivation vs. normal conditions, the library was prepared using the rRNA removal method. The libraries of other samples were prepared using the polyA enrichment method. All libraries were sequenced on the Illumina PE150 platform (Novogene). Triplicate samples were analyzed for cell culture-based RNA-seq, while mouse tissues collected from five individual mice were analyzed for each group during RNA-seq analysis. After obtaining the Fastq file, FastQC was used to perform pre-mapping sequencing quality evaluation. Then the sequencing reads were mapped to the hg38 human reference genome or mm10 mouse reference genome by HISAT2 with the default parameters. HTSeq was used to calculate the raw gene counts. DESeq2 was used to normalize and process the raw gene counts for differential gene expression analysis. Adjusted p -value was calculated using the Benjamini–Hochberg method to control for false discovery rate. The criteria for DEGs were as follows: for DEGs in HepG2 *LDLR* KO/*HMGCR* KO/*DKO* cells compared with vector, the cutoff was $|\text{fold change}| \geq 2$, mean read count ≥ 10 , $p\text{-value} \leq 0.05$ and $p.\text{adjust} \leq 0.05$; for DEGs in HeLa *LDLR* KO/*HMGCR* KO/*DKO* cells compared with vector, sterol depleted versus normal (vector), or *SREBF2* KO versus vector (sterol depleted), the cutoff was $|\text{fold change}| \geq 1.5$, mean read count ≥ 10 , $p\text{-value} \leq 0.05$ and $p.\text{adjust} \leq 0.05$; for DEGs in liver or brain of *Ggt7*^{-/-} mice compared with *Ggt7*^{+/+} mice, the cutoff was $|\text{fold change}| \geq 1.5$, mean read count ≥ 10 , $p\text{-value} \leq 0.05$ and $p.\text{adjust} \leq 0.25$. The p -value of Venn overlap was calculated in R by Fisher's exact test. The functional enrichment analysis of DEGs was

performed by GO and KEGG analysis with clusterProfiler R package. The volcano plot was generated by the ggplot2 R package.

Proteomics analysis

HepG2 cells (2×10^6) were seeded into one 15 cm dish, infected with sgRNA-containing lentiviral particles for *LDLR/HMGCR* DKO. Six days later, cells were washed twice with pre-chilled PBS, and dissolved in 500 μ L lysis buffer (6 M Urea, 0.1 M NaHCO₃, 0.2% SDS) plus protease inhibitor. The collected cell samples were further processed by Novogene company for mass spectrometry analysis. The separated peptides were analyzed by Q Exactive HF mass spectrometer (Thermo Fisher Scientific). The resulting spectra from each fraction were searched separately against the Uniprot database. Triplicate samples were analyzed for each group. Proteins with $|\text{FoldChange}| \geq 1.5$ and $p\text{-value} \leq 0.05$ are regarded as significant. A more stringent cutoff of $|\text{FoldChange}| \geq 1.5$ and $p\text{-value} \leq 0.01$ was also used.

Functional enrichment analysis

The functional enrichment analysis of gene hits was performed by gene ontology (GO) and Kyoto encyclopedia of genes and genomes (KEGG) analysis in clusterProfiler R package. The BP (Biological Process) module was used for GO analysis. Significant terms were defined with a cutoff of $p\text{-value} < 0.05$ and $q\text{-value} < 0.05$ for both GO and KEGG analysis.

Compiling candidate genes via human genetic variant analysis

Three sources of GWAS data were considered to compile the candidate genes associated with lipid disorders and cardiovascular diseases. For source 1, the GWAS meta-analysis results were accessed via five phenotypes or traits from the HuGeAMP database (<https://hugeamp.org>), including cholesterol, high-density lipoprotein, low-density lipoprotein, coronary artery disease, and myocardial infarction. HuGE (Human Genetic Evidence) scores quantify genetic support for the involvement of genes in the diseases or traits with a value ≥ 30 meaning very strong. We considered the genes with scores above 50 as the candidates of the current study. For source 2, a gene list linked to lipids was downloaded from the GWAS Catalog (EFO_0004529) and the cutoff was $p\text{-value} \leq 1E - 30$. Then we removed duplicate genes, miRNA, or lncRNA genes from the list to obtain the candidates of the current study. For source 3, twenty literatures were collected to comprehensively search the genes related to abnormal lipid metabolism. These published literatures cover the results of human genetic variants analysis spanning the following resources and types [20, 49–67]: (1) exome datasets from the Global Lipids Genetics Consortium (GLGC) and the UK Biobank (UKBB), as well as Million Veteran Program (MVP); (2) individual-level phenotype and genotype data from 66,240 individuals of European descent in 32 cohorts; (3) GWAS for coronary artery disease comprising 181,522 cases among 1,165,690 participants of predominantly European ancestry; (4) protein-coding genetic variants in 47,532 East Asian individuals using an exome array; (5) HuH7 LDL uptake regulators which are enriched for LDL GWAS associations; (6) GWAS in 34,541 CAD cases and 261,984 controls of UK Biobank resource followed by replication in 88,192 cases and 162,544 controls from CARDIoGRAMplusC4D; (7) analysis of

the population-specific differences of coronary artery disease between European and East Asian descents; (8) genome-wide association data from three studies ($n = 8816$ that included 2758 individuals from the Diabetes Genetics Initiative as well as 1874 individuals from the FUSION study of type 2 diabetes and 4184 individuals from the SardiNIA study; (9) GWAS results of metabolic traits in Finnish cohort; (10) GWAS analysis of loci affecting lipid traits sampled randomly from 16 population-based cohorts; (10) GWAS of 17 lipoprotein measures determined by NMR together with LDL-C, HDL-C, triglycerides, ApoA1, and ApoB in 17,296 women from the Women's Genome Health Study (WGHS); (12) peripheral blood RNA-seq data from 2116 unrelated individuals and systematically identified context-dependent eQTLs using a hypothesis-free strategy; and (13) 450,636 UK Biobank participants with dyslipoproteinemia subtypes. A non-redundant gene list was compiled from the three sources as candidate genes associated with lipid metabolism and related diseases with human genetic evidence (Additional file 6: Table S5).

Immunoblot analysis

Cell lysates or homogenized mouse tissues (approximately 20 mg) were prepared in RIPA buffer (Beyotime, P0013) with addition of PMSF (Beyotime, ST506) and incubated on ice for 10 min with frequent vortex and then centrifuged at 14,000 rpm for 10 min at 4 °C. Protein concentration was determined by bicinchoninic (BCA) protein assay (Meilunbio, MA0082). Protein supernatant was mixed with 5 × loading buffer and boiled at 95 °C for 5 min. Samples were resolved on 10% SDS-PAGE gels followed by transfer onto nitrocellulose filter membrane (Pall, C05-05002). Membranes were blocked with 5% milk in TBST buffer and incubated with primary antibody at 4 °C overnight in TBST buffer. Membranes were washed three times with TBST and incubated with secondary antibodies before proceeding to a chemiluminescent analyzer for band visualization. The following antibodies were used in this study: Rabbit monoclonal anti-HMGCR (Abcam, ab174830), Rabbit polyclonal anti-LDLR (Proteintech, 10785-1-AP), Rabbit polyclonal anti-GAPDH (Santa Cruz, sc-25778), Rabbit polyclonal anti-GGT7 (Proteintech, 24674-1-AP), Rabbit polyclonal anti-MYH10 (Proteintech, 19673-1-AP), Rabbit control IgG (Proteintech, 30000-0-AP), Mouse monoclonal anti-FLAG (Invitrogen, MA191878), Rabbit polyclonal anti-β actin (Invitrogen, PA1-16889), Goat anti-Rabbit IgG (H + L) Secondary Antibody (Invitrogen, 31460), and Rabbit anti-Mouse IgG (H + L) Secondary Antibody (Invitrogen, 31450).

Identification of GGT7-associated proteins

HepG2 cells cultured in 15 cm dishes were infected with lentiviruses expressing FLAG-GGT7. After 7 days, cells were solubilized with lysis buffer (TNE, 50 mM Tris HCl, pH 7.4, with 150 mM NaCl, 1 mM EDTA, and 1% Triton X-100, supplemented with protease inhibitor cocktail (Roche, 4693159001)). Protein lysates were extracted and incubated with Anti-DYKDDDDK Magnetic Agarose (Thermo Fisher Scientific, A36797) at 4 °C for 6 h. After washing with PBS, the bound proteins were eluted with 3 × FLAG peptide (Sangon, T510060-0005). The eluted samples were added to 5 × loading buffer and boiled at 95 °C for 5 min. The purified proteins were quantified using SDS-PAGE, followed by Coomassie blue staining. Proteins of the whole

lane in the gel were cut and analyzed by mass spectrometry (Novogene). Database searching of all raw data was performed using Proteome Discoverer 2.4 software (Thermo Fisher Scientific). Identified proteins were ranked in descending order by score, and more unique peptides indicated higher confidence. For validation of interaction between GGT7 and MYH10, HepG2 cells were lysed with TNE for 10 min on ice. The supernatant was incubated with 2 μ g control IgG, GGT7, or MYH10 antibody pre-incubated with Protein G agarose (Thermo Fisher Scientific, 10004D) at 4 °C overnight. The samples were washed with TNE for three times. The pellet was mixed with 2 \times loading buffer and boiled at 95 °C for 5 min, followed by immunoblot analysis with MYH10 and GGT7 antibodies.

Histological analysis

Mouse liver was collected and fixed with 4% paraformaldehyde for 36–48 h. After fixation, the samples were immersed in a 70% alcohol solution overnight. Gradient concentration of alcohol was used for dehydration. The dehydrated tissues were soaked into xylene and then into soft paraffin at 58 °C for 1.5 h as well as hard paraffin for 1.5 h. The tissues embedded in paraffin were cut into 5 μ m slices. All the paraffin was dissolved away with xylene and washed with several changes of gradient alcohol to remove the xylene. The slide was stained with hematoxylin for 5 min and then stained with eosin for 2 min. Following washing with different concentrations of alcohol, the slide was dissolved with xylene for 20 min and observed by LEICA DM4000 B LED microscope. For Oil Red O staining of lipid droplets, frozen liver samples were embedded in Tissue-Tek OCT compound (Sakura) and cut into 7 μ m. The sections were washed with 60% isopropanol for 5 min, and incubated with Oil Red O working solution for 30 min. Then the sections were stained with hematoxylin and the images were captured under a microscope (LEICA DM4000 B LED).

Blood and tissue sample analysis

Blood samples were collected and centrifuged at 3000 rpm for 10 min at 4 °C. The supernatant was directly used to detect serum total cholesterol (Nanjing Jiancheng Bioengineering Institute, A111-1-1), triglycerides (Nanjing Jiancheng Bioengineering Institute, A110-1-1), high-density lipoprotein cholesterol (HDL-C, Nanjing Jiancheng Bioengineering Institute, A112-1-1), low-density lipoprotein cholesterol (LDL-C, Nanjing Jiancheng Bioengineering Institute, A113-1-1), aspartate aminotransferase (AST, Nanjing Jiancheng Bioengineering Institute, C010-2-1), alanine aminotransferase (ALT, Nanjing Jiancheng Bioengineering Institute, C009-2-1) and γ -glutamyltransferase (GGT, Nanjing Jiancheng Bioengineering Institute, C017-2-1) according to manufacturer's instructions. To measure the lipid (cholesterol, triglycerides, HDL-C, and LDL-C) levels of the liver and brain, snap-frozen samples were weighed (~40 mg) and homogenized in chloroform:methanol (2:1; v/v) mixture and vigorously vortexed for 20 s. The lower organic phase was collected and dried. Use 200 μ L of 1% Triton X-100 in ethanol to dissolve the samples. Triglycerides and cholesterol content were determined using the enzymatic reagents based on the manufacturer's instructions as above.

Quantification and statistical analysis

Statistical details of experiments can be found in the figure legends. Statistical analysis was performed using GraphPad Prism (version 9.5.1), MAGeCK (version 0.5.9.2), or R (version 4.2.3). All values are reported as Mean \pm SD. Data were analyzed using a two-tailed unpaired *t* test, one-way ANOVA with Tukey's, and Dunnett's tests where appropriate. Asterisks indicate **p* < 0.05, ***p* < 0.01, and ****p* < 0.001.

Supplementary Information

The online version contains supplementary material available at <https://doi.org/10.1186/s13059-025-03531-8>.

Additional file 1. Supplementary figures S1 to S7. Includes supplementary figures and the legends for Fig. S1 to S7

Additional file 2. Table S1. CRISPR screen data

Additional file 3. Table S2. Metabolomic profiling data

Additional file 4. Table S3. RNA-seq data

Additional file 5. Table S4. Proteomics data

Additional file 6. Table S5. Data of human genetic variant analysis

Additional file 7. Table S6. Oligonucleotides and primer sequences

Additional file 8. Uncropped images for the blots

Acknowledgements

Not applicable.

Peer review information

Wenjing She was the primary editor of this article and managed its editorial process and peer review in collaboration with the rest of the editorial team. The peer-review history is available in the online version of this article.

Authors' contributions

T.F. conceived the study and designed the research. H.S. conducted most of the experiments and bioinformatic analysis. T.F. wrote the manuscript with input from H.S. T.F. supervised the study. All authors read and approved the final manuscript.

Funding

This work was supported by the Fundamental Research Funds for the Central Universities (N182005005), the 111 Project (B16009), the Construction Project of Liaoning Provincial Key Laboratory, China (2022JH13/10200026) and Liaoning Revitalization Talents Program (XLYC1807212) to T.F.

Data availability

The raw sequencing data for CRISPR screening and RNA-seq generated in this study have been deposited and are publicly available in the Genome Sequence Archive in the National Genomics Data Center, China National Center for Bioinformation / Beijing Institute of Genomics, Chinese Academy of Sciences, under accession code (GSA-Human: HRA007196 [68], GSA: CRA016018 [69]) at <https://ngdc.cncb.ac.cn/>. The mass spectrometry proteomics data have been deposited to the ProteomeXchange Consortium via the PRIDE partner repository with the dataset identifier PXD052324 [70] at <https://www.ebi.ac.uk/pride>.

Declarations

Ethics approval and consent to participate

All animal care and experimental procedures used in this study were approved by the Animal Care and Use Committee of Northeastern University (NEU-EC-2021A019S), according to national and institutional guidelines.

Consent for publication

Not applicable.

Competing interests

The authors declare no competing interests.

Received: 7 August 2024 Accepted: 6 March 2025

Published online: 17 March 2025

References

- Chen L, Chen XW, Huang X, Song BL, Wang Y, Wang Y. Regulation of glucose and lipid metabolism in health and disease. *Sci China Life Sci.* 2019;62:1420–58.
- Luo J, Yang H, Song BL. Mechanisms and regulation of cholesterol homeostasis. *Nat Rev Mol Cell Biol.* 2020;21:225–45.
- Porter JA, Young KE, Beachy PA. Cholesterol modification of hedgehog signaling proteins in animal development. *Science.* 1996;274:255–9.
- Xiao X, Tang JJ, Peng C, Wang Y, Fu L, Qiu ZP, et al. Cholesterol modification of smoothened is required for hedgehog signaling. *Mol Cell.* 2017;66(154–162): e10.
- Zhao D, Liu J, Wang M, Zhang X, Zhou M. Epidemiology of cardiovascular disease in China: current features and implications. *Nat Rev Cardiol.* 2019;16:203–12.
- Zhao D, Liu J, Xie W, Qi Y. Cardiovascular risk assessment: a global perspective. *Nat Rev Cardiol.* 2015;12:301–11.
- Brown MS, Radhakrishnan A, Goldstein JL. Retrospective on cholesterol homeostasis: the central role of scap. *Annu Rev Biochem.* 2018;87:783–807.
- Wang JQ, Li LL, Hu A, Deng G, Wei J, Li YF, et al. Inhibition of ASGR1 decreases lipid levels by promoting cholesterol excretion. *Nature.* 2022;608:413–20.
- Lu XY, Shi XJ, Hu A, Wang JQ, Ding Y, Jiang W, et al. Feeding induces cholesterol biosynthesis via the mTORC1-USP20-HMGR axis. *Nature.* 2020;588:479–84.
- Zhang YY, Fu ZY, Wei J, Qi W, Baituola G, Luo J, et al. A LIMA1 variant promotes low plasma LDL cholesterol and decreases intestinal cholesterol absorption. *Science.* 2018;360:1087–92.
- Chu BB, Liao YC, Qi W, Xie C, Du X, Wang J, et al. Cholesterol transport through lysosome-peroxisome membrane contacts. *Cell.* 2015;161:291–306.
- Wang JK, Li Y, Zhao XL, Liu YB, Tan J, Xing YY, et al. Ablation of plasma prekallikrein decreases low-density lipoprotein cholesterol by stabilizing low-density lipoprotein receptor and protects against atherosclerosis. *Circulation.* 2022;145:675–87.
- Jiang SY, Yang X, Yang Z, Li JW, Xu MQ, Qu YX, et al. Discovery of an insulin-induced gene binding compound that ameliorates nonalcoholic steatohepatitis by inhibiting sterol regulatory element-binding protein-mediated lipogenesis. *Hepatology.* 2022;76:1466–81.
- Han F, Liu X, Chen C, Liu Y, Du M, Zhou Y, et al. Hypercholesterolemia risk-associated GPR146 is an orphan G-protein coupled receptor that regulates blood cholesterol levels in humans and mice. *Cell Res.* 2020;30:363–5.
- Yu H, Rimbert A, Palmer AE, Toyohara T, Xia Y, Xia F, et al. GPR146 deficiency protects against hypercholesterolemia and atherosclerosis. *Cell.* 2019;179(1276–1288):e14.
- Nishiga M, Liu C, Qi LS, Wu JC. The use of new CRISPR tools in cardiovascular research and medicine. *Nat Rev Cardiol.* 2022;19:505–21.
- Wang JY, Doudna JA. CRISPR technology: a decade of genome editing is only the beginning. *Science.* 2023;379:eadd8643.
- Shan H, Fei T. CRISPR screening in cardiovascular research. *Front Cell Dev Biol.* 2023;11:1175849.
- Emmer BT, Hesketh GG, Kotnik E, Tang VT, Lascuna PJ, Xiang J, et al. The cargo receptor SURF4 promotes the efficient cellular secretion of PCSK9. *Elife.* 2018;7:7.
- Emmer BT, Sherman EJ, Lascuna PJ, Graham SE, Willer CJ, Ginsburg D. Genome-scale CRISPR screening for modifiers of cellular LDL uptake. *PLoS Genet.* 2021;17:e1009285.
- Lu A, Hsieh F, Sharma BR, Vaughn SR, Enrich C, Pfeffer SR. CRISPR screens for lipid regulators reveal a role for ER-bound SNX13 in lysosomal cholesterol export. *J Cell Biol.* 2022;221:e202105060.
- Lucero D, Dikilitas O, Mendelson MM, Aligabi Z, Islam P, Neufeld EB, et al. Transgelin: a new gene involved in LDL endocytosis identified by a genome-wide CRISPR-Cas9 screen. *J Lipid Res.* 2022;63:100160.
- Menzies SA, Volkmar N, Van Den Boomen DJ, Timms RT, Dickson AS, Nathan JA, et al. The sterol-responsive RNF145 E3 ubiquitin ligase mediates the degradation of HMG-CoA reductase together with gp78 and Hrd1. *Elife.* 2018;7:7.
- Smith GA, Padmanabhan A, Lau BH, Pampana A, Li L, Lee CY, et al. Cold shock domain-containing protein E1 is a posttranscriptional regulator of the LDL receptor. *Sci Transl Med.* 2022;14:eabj8670.
- Xiao J, Xiong Y, Yang LT, Wang JQ, Zhou ZM, Dong LW, et al. POST1/C12ORF49 regulates the SREBP pathway by promoting site-1 protease maturation. *Protein Cell.* 2021;12:279–96.
- Van Den Boomen DJH, Sienkiewicz A, Berlin I, Jongasma MLM, Van Elstrand DM, Luzio JP, et al. A trimeric Rab7 GEF controls NPC1-dependent lysosomal cholesterol export. *Nat Commun.* 2020;11:5559.
- Hamilton MC, Fife JD, Akinci E, Yu T, Khowpinitchai B, Cha M, et al. Systematic elucidation of genetic mechanisms underlying cholesterol uptake. *Cell Genom.* 2023;3:100304.
- Khan TG, Cunha JB, Raut C, Burroughs M, Goonewardena SN, Smrcka AV, et al. Functional interrogation of cellular Lp(a) uptake by genome-scale CRISPR screening. *bioRxiv.* 2024. <https://doi.org/10.1101/2024.05.11.593568>.
- Wang B, Wang M, Zhang W, Xiao T, Chen CH, Wu A, et al. Integrative analysis of pooled CRISPR genetic screens using MAGECKFlute. *Nat Protoc.* 2019;14:756–80.
- Enkler L, Spang A. Functional interplay of lipid droplets and mitochondria. *FEBS Lett.* 2024;598:1235–51.
- Graham A. Mitochondrial regulation of macrophage cholesterol homeostasis. *Free Radic Biol Med.* 2015;89:982–92.
- Heisterkamp N, Groffen J, Warburton D, Sneddon TP. The human gamma-glutamyltransferase gene family. *Hum Genet.* 2008;123:321–32.
- Tan C, Zhang H, Yu D, Hu Y, Wang P, Wang D, et al. A genome-wide association study identifies novel association between genetic variants in GGT7 and LINC00944 and hypertension. *Clin Transl Med.* 2021;11:e388.
- Azarova I, Klyosova E, Polonikov A. The link between type 2 diabetes mellitus and the polymorphisms of glutathione-metabolizing genes suggests a new hypothesis explaining disease initiation and progression. *Life (Basel).* 2021;11:11.
- Mason JE, Starke RD, Van Kirk JE. Gamma-glutamyl transferase: a novel cardiovascular risk biomarker. *Prev Cardiol.* 2010;13:36–41.

36. Barthelson K, Newman M, Lardelli M. Sorting out the role of the sortilin-related receptor 1 in Alzheimer's disease. *J Alzheimers Dis Rep.* 2020;4:123–40.
37. Smith GS, Walter GL, Walker RM. Clinical pathology in non-clinical toxicology testing. In: Haschek and Rousseaux's Handbook of Toxicologic Pathology. 2013;565–94. <https://doi.org/10.1016/B978-0-12-415759-0.00018-2>.
38. Bui TT, Nitta RT, Kahn SA, Razavi SM, Agarwal M, Aujla P, et al. gamma-Glutamyl transferase 7 is a novel regulator of glioblastoma growth. *BMC Cancer.* 2015;15:225.
39. Wang X, Zhang L, Chan FKL, Ji J, Yu J, Liang JQ. Gamma-glutamyltransferase 7 suppresses gastric cancer by cooperating with RAB7 to induce mitophagy. *Oncogene.* 2022;41:3485–97.
40. Bharani V, Ramesh V, Rao RN, Tewari S. Evaluation of gamma glutamyl transferase as a marker of cardiovascular risk, in 200 angiographically proven coronary artery disease patients. *Indian Heart J.* 2017;69:325–7.
41. Bobrus-Chociej A, Flisiak-Jackiewicz M, Daniluk U, Wojtkowska M, Klusek-Oksiuta M, Tarasow E, et al. Estimation of gamma-glutamyl transferase as a suitable simple biomarker of the cardiovascular risk in children with non-alcoholic fatty liver disease. *Acta Biochim Pol.* 2018;65:539–44.
42. Han KS, Cho DY, Kim YS, Kim KN. Serum gamma-glutamyl transferase concentration within the reference range is related to the coronary heart disease risk prediction in Korean men: analysis of the Korea National Health and Nutrition Examination Survey (V-1, 2010 and V-2, 2011). *Chin Med J (Engl).* 2015;128:2006–11.
43. Mao Y, Qi X, Xu W, Song H, Xu M, Ma W, et al. Serum gamma-glutamyl transferase: a novel biomarker for coronary artery disease. *Med Sci Monit.* 2014;20:706–10.
44. Xing M, Gao M, Li J, Han P, Mei L, Zhao L. Characteristics of peripheral blood Gamma-glutamyl transferase in different liver diseases. *Medicine (Baltimore).* 2022;101:e28443.
45. Gong S, Gan S, Zhang Y, Zhou H, Zhou Q. Gamma-glutamyl transferase to high-density lipoprotein cholesterol ratio is a more powerful marker than TyG index for predicting metabolic syndrome in patients with type 2 diabetes mellitus. *Front Endocrinol (Lausanne).* 2023;14:1248614.
46. Kasapoglu B, Turkay C, Yalcin KS, Carlioglu A, Kakteker A. Role of gamma-glutamyl transferase levels in prediction of high cardiovascular risk among patients with non-alcoholic fatty liver disease. *Indian J Med Res.* 2016;143:30–6.
47. Celik O, Cakmak HA, Satilmis S, Gungor B, Akin F, Ozturk D, et al. The relationship between gamma-glutamyl transferase levels and coronary plaque burdens and plaque structures in young adults with coronary atherosclerosis. *Clin Cardiol.* 2014;37:552–7.
48. Cariou B, Le Bras M, Langhi C, Le May C, Guyomarc'h-Delasalle B, Krempf M, et al. Association between plasma PCSK9 and gamma-glutamyl transferase levels in diabetic patients. *Atherosclerosis.* 2010;211:700–2.
49. Aragam KG, Jiang T, Goel A, Kanoni S, Wolford BN, Atri DS, et al. Discovery and systematic characterization of risk variants and genes for coronary artery disease in over a million participants. *Nat Genet.* 2022;54:1803–15.
50. Asselbergs FW, Guo Y, Van Iperen EP, Sivapalaratnam S, Tragante V, Lanktree MB, et al. Large-scale gene-centric meta-analysis across 32 studies identifies multiple lipid loci. *Am J Hum Genet.* 2012;91:823–38.
51. Aulchenko YS, Ripatti S, Lindqvist I, Boomsma D, Heid IM, Pramstaller PP, et al. Loci influencing lipid levels and coronary heart disease risk in 16 European population cohorts. *Nat Genet.* 2009;41:47–55.
52. Chasman DI, Pare G, Mora S, Hopewell JC, Peloso G, Clarke R, et al. Forty-three loci associated with plasma lipoprotein size, concentration, and cholesterol content in genome-wide analysis. *PLoS Genet.* 2009;5:e1000730.
53. Gilliland T, Dron JS, Selvaraj MS, Trinder M, Paruchuri K, Urbut SM, et al. Genetic architecture and clinical outcomes of combined lipid disturbances. *Circ Res.* 2024;135:265–76.
54. Hu Y, Qiu S, Cheng L. Integration of multiple-omics data to analyze the population-specific differences for coronary artery disease. *Comput Math Methods Med.* 2021;2021:7036592.
55. Kathiresan S, Melander O, Guiducci C, Surti A, Burtt NP, Rieder MJ, et al. Six new loci associated with blood low-density lipoprotein cholesterol, high-density lipoprotein cholesterol or triglycerides in humans. *Nat Genet.* 2008;40:189–97.
56. Kathiresan S, Willer CJ, Peloso GM, Demissie S, Musunuru K, Schadt EE, et al. Common variants at 30 loci contribute to polygenic dyslipidemia. *Nat Genet.* 2009;41:56–65.
57. Klarin D, Damrauer SM, Cho K, Sun YV, Teslovich TM, Honerlaw J, et al. Genetics of blood lipids among ~300,000 multi-ethnic participants of the million veteran program. *Nat Genet.* 2018;50:1514–23.
58. Liu DJ, Peloso GM, Yu H, Butterworth AS, Wang X, Mahajan A, et al. Exome-wide association study of plasma lipids in >300,000 individuals. *Nat Genet.* 2017;49:1758–66.
59. Lu X, Peloso GM, Liu DJ, Wu Y, Zhang H, Zhou W, et al. Exome chip meta-analysis identifies novel loci and East Asian-specific coding variants that contribute to lipid levels and coronary artery disease. *Nat Genet.* 2017;49:1722–30.
60. Nikpay M, Goel A, Won HH, Hall LM, Willenborg C, Kanoni S, et al. A comprehensive 1,000 genomes-based genome-wide association meta-analysis of coronary artery disease. *Nat Genet.* 2015;47:1121–30.
61. Sabatti C, Service SK, Hartikainen AL, Pouta A, Ripatti S, Brodsky J. Genome-wide association analysis of metabolic traits in a birth cohort from a founder population. *Nat Genet.* 2009;41:35–46.
62. Schunkert H, König IR, Kathiresan S, Reilly MP, Assimes TL, Holm H, et al. Large-scale association analysis identifies 13 new susceptibility loci for coronary artery disease. *Nat Genet.* 2011;43:333–8.
63. Teslovich TM, Musunuru K, Smith AV, Edmondson AC, Stylianou IM, Koseki M, et al. Biological, clinical and population relevance of 95 loci for blood lipids. *Nature.* 2010;466:707–13.
64. Van Der Harst P, Verweij N. Identification of 64 novel genetic loci provides an expanded view on the genetic architecture of coronary artery disease. *Circ Res.* 2018;122:433–43.
65. Willer CJ, Sanna S, Jackson AU, Scuteri A, Bonnycastle LL, Clarke R, et al. Newly identified loci that influence lipid concentrations and risk of coronary artery disease. *Nat Genet.* 2008;40:161–9.
66. Willer CJ, Schmidt EM, Sengupta S, Peloso GM, Gustafsson S, Kanoni S, et al. Discovery and refinement of loci associated with lipid levels. *Nat Genet.* 2013;45:1274–83.
67. Zernakova DV, Deelen P, Vermaat M, Van Iterson M, Van Galen M, Arindrarto W, et al. Identification of context-dependent expression quantitative trait loci in whole blood. *Nat Genet.* 2017;49:139–45.

68. Fei T. Integrative multi-omics identifies Gamma-glutamyltransferase GGT7 as a regulator of cholesterol metabolism (HRA007196). Genome sequence archive. National Genomics Data Center. 2024. <https://ngdc.cncb.ac.cn/gsa-human/browse/HRA007196>.
69. Fei T. Integrative multi-omics identifies Gamma-glutamyltransferase GGT7 as a regulator of cholesterol metabolism (CRA016018). Genome sequence archive. National Genomics Data Center. 2024. <https://ngdc.cncb.ac.cn/gsa/browse/CRA016018>.
70. Fei T. LDLR and HMGCR double knock out human HepG2 cells LC-MSMS. PRIDE PRoteomics IDEntifications Archive. 2024. <https://www.ebi.ac.uk/pride/archive/projects/PXD052324>.

Publisher's Note

Springer Nature remains neutral with regard to jurisdictional claims in published maps and institutional affiliations.